
Article:
Zhu, Z.Q. orcid.org/0000-0001-7175-3307, Khatab, M.F., Li, H. et al. (1 more author) (2018) A novel axial flux magnetically geared machine for power split application. IEEE Transactions on Industry Applications, 54 (6). pp. 5954-5966. ISSN 0093-9994

https://doi.org/10.1109/TIA.2018.2859173

A Novel Axial Flux Magnetically Geared Machine for Power Split Application

Z.Q. Zhu, *Fellow, IEEE*, Mohammed F. Khatab, H. Y. Li, and Y. Liu

***Abstract* - This paper proposes an axial flux magnetically geared (AFMG) permanent magnet (PM) machine for power split application in hybrid electric vehicles (HEVs). The proposed AFMG machine has the merits of simple structure and improved torque density by combining a magnetic gear (MG) with a PM machine. The machine can realize power split with the help of dual mechanical ports and one electrical port, i.e., the input mechanical power and/or electrical power produced by the machine can be split or integrated. The operation principle and two feasible stator slot/rotor pole combinations are analyzed. Moreover, the influence of the machine parameters on the output torque as well as the performance of both combinations are investigated and compared by using JMAG three dimensional (3D) finite element analysis (FEA). In addition, the method of boosting the machine torque is described and experiment results of the proposed machine prototype are provided and compared with FEA results.**

***Index Terms*: Axial flux machines, magnetic gears, magnetically geared machines, power split.**

I. Introduction

AXIAL flux permanent magnet (AFPM) machines have attracted significant research attention. They have several unique advantages over radial flux PM (RFPM) machines such as high torque density, low rotor losses, and high efficiency [1].

In many industrial applications, mechanical gears are widely used for delivering torque and speed from the prime-mover to other rotating components [2]. However, due to the physical contact, frequent maintenance, high friction losses, large vibration and noise are inevitable. Therefore, magnetic gears (MGs) are currently being developed in an attempt to replace mechanical gears, due to their feature of contactless transmission [3]. The development of MG topologies in which modulation rings are located between the two rotors inspires researchers to create new types of cascaded electrical machines (i.e. magnetically geared machines) where the MGs are integrated with permanent magnet machines under the same frame [4].

With the merit of high efficiency, fuel economy and low emission, hybrid electric vehicles (HEVs) have been regarded as the most realistic substitute for conventional fuel vehicles [5]. In HEVs, a mechanical planetary gear is always adopted to transmit and split the power produced by an internal combustion engine (ICE) [6]. However, planetary gears have the same problems as conventional mechanical gears, namely, lubrication and mechanical loss. To eliminate the use of planetary gears, magnetically geared machines are now being widely investigated for HEVs, with the potential of achieving power split function.

The authors are with the Department of Electronic and Electrical Engineering, University of Sheffield, Sheffield S1 4DE, UK. (E-mail: z.q.zhu@sheffield.ac.uk; mfhkhatab1@sheffield.ac.uk; hli53@sheffield.ac.uk; vliu147@sheffield.ac.uk.

Numerous radial-flux magnetically geared machine topologies have been proposed [7], [8], and several topologies have been particularly invented for power split in HEVs, as presented in [9], [10]. In addition, axial flux magnetically geared PM (AFMGPM) machine topologies for various applications have been presented and analyzed. An axial flux magnetically geared machine with torque density of approximately 15 kNm/m^3 was firstly presented in [11]. Then, several other AFMGPM topologies were proposed and analyzed for wind power applications [12-14]. Furthermore, AFPM machine topologies have also been proposed to realize power split function and have the merit of high torque density and short axial space compared to their radial counterparts. AFPM machines have been introduced to realize power split function in HEVs and wind power applications [15], [16]. Nevertheless, these axial flux machines have not attracted as much research attention as the radial counterparts [14]. To the author's knowledge, only one AFMGPM machine topology has been presented for power split applications in HEVs. In [17], an axial flux magnetically geared machine is presented for HEVs, in which a double stator with distribution windings has been utilized. However, the machine has a complex structure and low power factor in generating and motoring modes.

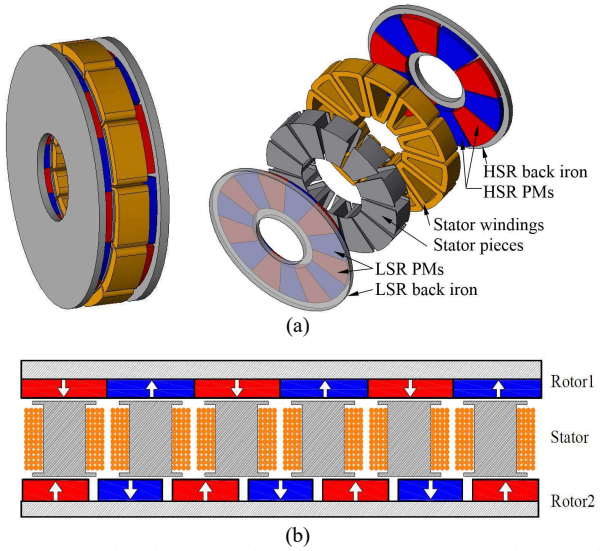

Fig. 1 3D model of the proposed machine topology. (a) 3D and exploded view. (b) 2D cross section at average diameter.

In this paper, a new 3-phase AFMGPM machine for power split application is proposed, of which the basic concept is presented in [18] and [19]. The topology is a combination of a high performance yokeless and segmented armature machine, as presented in [20], [21], and an axial MG, which shares the machine stator as modulation ring. It should be noted that the distinct feature of the proposed machine is that the fractional slot concentrated winding is utilised to amplify the torque of both PM rotors with different pole-pair numbers. By utilizing JMAG designer 3D-FEA [22], possible rotor pole combinations of the proposed topology at stator pole of 12 are analyzed and compared. The machine

performance at no-load and full-load is also studied. The last section describes the prototype design and experimental validation is also conducted.

II. Proposed Axial Flux MG Machine and Principle of Operation

Fig. 1 shows the proposed machine topology. The machine is comprised of two surface mounted PM axial rotors and one stator constructed of a combination of iron pieces with concentrated windings. By employing different pole-pair numbers for two PM rotors, a magnetic gearing effect can be exhibited within both rotors. Moreover, the utilized concentrated windings are wound over each stator piece. The principle of operation and gearing ratio of MGs are derived and described in [23]. The power can be transferred between the high-speed rotor (HSR) and low-speed rotor (LSR) when the relationship between both rotor pole pairs and modulator piece poles n_s is

$$n_s = p_l + p_h \tag{1}$$

The corresponding gearing ratio G_r with fixed modulator pieces can be calculated as follows:

$$G_r = -\frac{p_l}{p_h} = \frac{T_l}{T_h} = \frac{n_h}{n_l} \tag{2}$$

where p_l, T_l and n_l are pole pairs, torque and rotational speed of the LSR, respectively. p_h, T_h and n_h are pole pairs, torque and rotational speed of the HSR, respectively.

In addition to the torque exerted on both rotors due to the MG effect, the torque produced by the interaction between armature current flux harmonics and PM flux harmonics is utilized to increase the total machine torque. For the magnetically geared machine proposed in this paper, the stationary pole pieces n_s is chosen as 12, and several rotor pole combinations can be considered according to the MG principle given in (1). In addition, for PM machines, the relationship between the stator slots n_s and the rotor pole pairs p can be given by

$$2p = n_s \pm k, \; k = 1,2, \ldots \tag{3}$$

Therefore, by considering both (1) and (3), possible rotor pole combinations of the machine can be determined for n_s of 12 and are listed in Table I. However, for the machines with concentrated windings, the stator slots n_s and rotor pole 2 p combinations largely affect winding factor and performance [24], [25].

For PM machines, the number of slots per pole per phase (S_{pp}) is defined by

$$S_{pp} = \frac{n_s}{2pm} \tag{4}$$

where m is the number of phases [26].The fundamental winding factors K_{w1} of concentrated windings for possible rotor pole combinations are then calculated and listed in Table I. Due to the relatively high winding factor, for the proposed AFMGPM machine, the concentrated winding is suggested for two rotor pole combinations. The first combination is known as (MG12/5-7), in which HSR pole pairs p_h equals 5 and LSR pole pairs p_l equals 7. The second combination is known as (MG12/4-8), in which p_h=4 and p_l=8. The remaining pole combinations in Table I are not suitable for the proposed topology since the S_{pp} of HSR is an integer, thus resulting in a low winding factor for concentrated windings. For the selected rotor pole combinations, the phase coils are connected in series and their winding EMF phasors are depicted in Fig.2.

TABLE I
ROTOR POLE COMBINATIONS FOR 3 PHASE CONCENTRATED WINDINGS.

n_s	p_l	p_h	G_r	K_{w1}		S_{pp}	
				LSR	HSR	LSR	HSR
12	7	5	1.4	0.933	0.933	4/7	2/5
	8	4	2	0.866	0.866	1/4	1/2
	10	2	5	0.50	0.50	1/5	1
	11	1	11	0.25	0.25	2/11	2

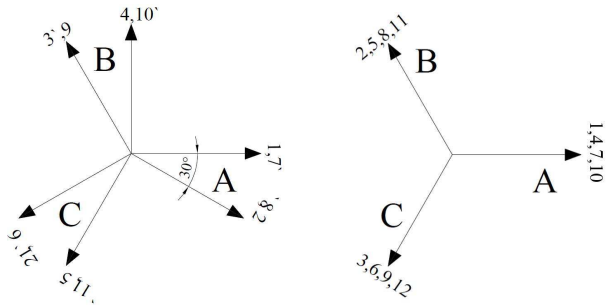

(a) (b)

Fig.2 Coil EMF phasors for proposed topologies. (a) MG12/5-7. (b) MG12/4-8.

III. Proposed System of Axial Flux Magnetically Geared Machine.

There are three types of HEV drive mode; series hybrid, parallel hybrid and power split [27]. For the series hybrid mode, the electric motor fed by the battery is directly applied to the wheels. The ICE is connected to the electric generator, which is used to charge the battery. The parallel hybrid mode is applied when both ICE and the electric machine are used to drive the wheels individually. The electric machine is utilized as a generator to charge the battery when the wheel is driven by the ICE. The power split mode is a combination between the above mentioned two modes, utilizing a planetary gear as a power split device.

The presented machine is proposed for variable speed HEV systems. The machine can realize the function of planetary gear and conventional synchronous motor/generator in conventional hybrid electric traction systems. The proposed machine operating condition can be classified into two operating modes, as can be seen in Fig.3.

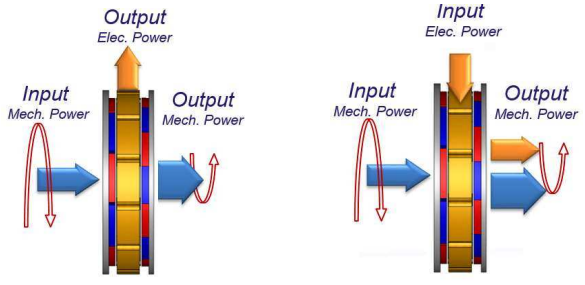

(a) (b)

Fig.3 Proposed machine operating modes. (a) Power split. (b) Magnetically geared motor.

1. Power split mode (Mode 1): In this case, either LSR or HSR is connected to the load, which is driven by the torque transferred due to the magnetic gearing effect from the input mechanical torque. The MG machine in this case operates as an MG to scale up/down the torque/speed of the prime-

mover. Moreover, the machine also operates as a generator due to the induced EMF on the stator windings (Fig.3-a).

2. Magnetically geared motor mode (Mode 2): In this operating mode, the load is driven by the torque transferred from the mechanical prime-mover utilizing a magnetic gearing effect. In addition, the machine torque can be amplified by the electromagnetic torque produced by armature reaction when the rated current is applied into the machine windings (Fig.3-b).

IV. Influence of Critical Parameters on Machine Performance

With the aim of obtaining the maximum torque transmission capability, the proposed AFMGPM machine is globally optimized by utilizing ANSYS Maxwell 2D-FEA software. Moreover, with the optimal dimensions, the influence of each parameter on machine performance is studied with the aid of JMAG 3D-FEA software. For this study, the machine is operated as a magnetically geared motor (mode2) and the LSR is assumed to be the output rotor which is connected to the drive, and the HSR is assumed as being connected to an external prime-mover. During the study process, the machine's constant parameters and dimensions are obtained and are provided in Table II. Meanwhile, the variable parameters are indicated in Fig. 4 and identified in Table III. It should be noted that the HSR speeds of both topologies are set as 400 rpm, and therefore, the LSR speeds are calculated according to (2). In this case, the frequency of the no-load and on-load stator fluxes f can be obtained by

$$f = \frac{n_h p_h}{60} = \frac{n_l p_l}{60} \tag{5}$$

Therefore, the stator flux frequency of MG12/5-7 is 33.33 Hz and it is 26.66 Hz for MG12/4-8.

TABLE II
CONSTANT PARAMETERS OF THE MACHINES.

Parameter	MG 12/5-7	MG 12/4-8
HSR rated speed (rpm)	400	400
LSR rated speed (rpm)	285.7	200
HSR pole pair no. (p_h)	5	4
LSR pole pair no. (p_l)	7	8
Stator slot number (n_s)	12	12
Machine outer diameter (mm)	90	90
Axial length (mm)	25	25
Air-gap length (mm)	0.5	0.5
Number of turns /phase	80	80
Packing factor	0.5	0.5
Copper loss (W)	30	30
Gearing ratio G_r	1.4	2
PM remanence B_r (T)	1.2	

Since it has been stated that the maximum torque can be produced by MG effect when the relative angle between the two rotors is adjusted at 90 elec. deg. [28], before starting the study procedure, the relative initial position between the two rotors must be adjusted at maximum torque position. Moreover, the stator winding is supplied by 3-phase currents. The current angle is adjusted to maximize the LSR torque in which the torque produced by armature reaction is added to the LSR MG torque. Consequently, since the AFMGPM has two torque parts, the influence of each parameter is exerted on the magnetic gear effect torque as well as the armature current torque.

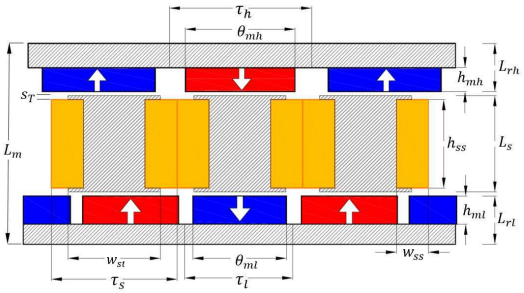

Fig. 4 Machine topology dimensions.

The sequence of the influence of the PM dimensions, slot width, tooth tip thickness, slot opening width, and the ratio between the inner and outer diameters on the machine torque is considered. Moreover, under the investigation of each individual parameter, the optimal values of other parameters will be fixed. The influence of each parameter on average torque is explained in the following section.

TABLE III
VARIABLE PARAMETERS OF THE MACHINES

Parameter	Symbol	Definition
HSR magnet angle ratio	r_{hp_ratio}	$\frac{\theta_{mh}}{\tau_h}$
LSR magnet angle ratio	r_{lp_ratio}	$\frac{\theta_{ml}}{\tau_l}$
HSR magnet thickness ratio	r_{ht_ratio}	$\frac{h_{mh}}{L_{rh}}$
LSR magnet thickness ratio	r_{lt_ratio}	$\frac{h_{ml}}{L_{rl}}$
Stator slot width ratio	s_{p_ratio}	$\frac{w_{ss}}{\tau_s}$
Stator slot tips thickness ratio	s_{T_ratio}	$\frac{s_T}{L_s}$
Stator tooth width ratio	s_{so_ratio}	$\frac{w_{st}}{\tau_s}$

A. Influence of PM dimensions

As can be seen in Fig. 4, the AFMGPM machine has high and low-speed rotors. By keeping other parameters constant, the influence of the LSR PM dimensions on the LSR average torque of MG12/5-7 and MG12/4-8 is illustrated in Fig. 5.
It is obvious that the maximum output torque is sensitive to the PM dimensions of both machines. A maximum LSR torque of MG12/5-7 can be obtained when the low-speed PM angle ratio r_{lp_ratio} is designed as (0.98-1) and the magnet thickness ratio r_{lt_ratio} is approximately 0.58, Fig. 5(a). On the other hand, the output torque of MG12/4-8 can be maximized when the LSR PM angle ratio is approximately 1 and the thickness ratio is approximately 0.5, Fig. 5(b).

Moreover, with optimal dimensions of LSR PM, the variation of high-speed PM dimensions on the output torque of two machine models is shown in Fig. 6. For MG12/5-7, the LSR torque reaches maximum value when the HSR PM thickness ratio r_{ht_ratio} and magnet angle ratio r_{hp_ratio} are designed at approximately 0.5 and 0.94, respectively, as can be seen in Fig. 6(a), whereas the torque of MG12/4-8 reaches maximum value when the HSR PM thickness ratio r_{ht_ratio} is approximately 0.5 and magnet angle ratio r_{hp_ratio} is approximately 0.87, Fig. 6(b). According to the obtained performances of the two topologies, the torque always reaches its maximum value when the rotor pole pitch and the stator pole pitch are approximately the same. The effect of leakage

flux is decreased in this case in which the MG torque is highly affected by the magnet angle.

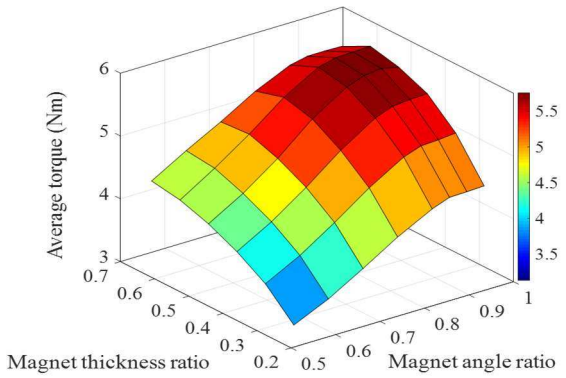

(a)

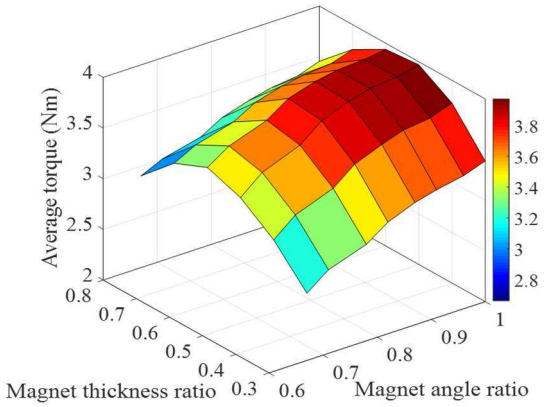

(b)

Fig. 5 Influen-ce of the LSR magnet dimensions on LSR output torque (a) MG12/5-7 (b) MG12/4-8.

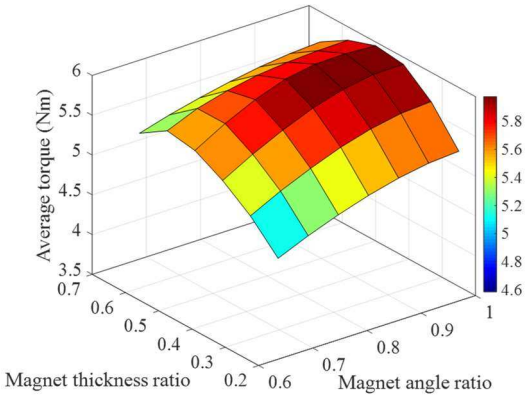

(a)

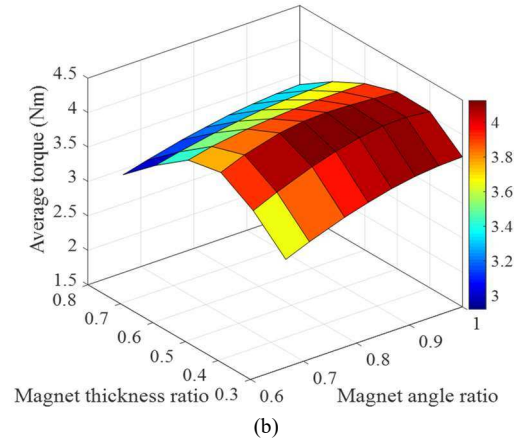

(b)

Fig. 6 Influence of HSR magnet dimensions on LSR output torque (a) MG12/5-7 (b) MG12/4-8.

B. *Influence of slot width*

The influence of the stator slot width was investigated, with the armature reaction at rated current being considered. The rated current can be calculated at fixed copper loss of 30 W. The machine current can be calculated by

$$I_{a\,RMS} = \sqrt{\frac{P_{cu}}{3\,R_a}} = \sqrt{\frac{P_{cu}\;\;A_a\;k_{pf}}{6\rho\;L_a N_a^2}} \tag{6}$$

where $I_{a\,RMS}$ is the RMS phase current, P_{cu} is the copper loss, R_a is the winding resistance, ρ is the copper resistivity, L_a is the stator active length, N_a is the number of winding turns per phase, k_{pf} is the winding packing factor and A_a is the coil area.

Fig. 7 indicates the effect of the slot width on the average torque for the considered models. It can be seen that the two topologies have optimal LSR average torque when the slot width ratio s_{p_ratio} is approximately 0.24. At fixed machine outer diameter, and by considering the end winding thickness, the machine active length in the radial direction is changed with the stator slot. The slot width in this case affects the torque produced by the armature reaction and MG effect.

C. *Influence of slot tip thickness*

At fixed stator width L_s, the average output torque for different tooth tip thicknesses is presented in Fig. 8. It can be seen that the average torque is sensitive to the stator width in which the torque decreases as the tooth tip thickness increases. That is due to the decreases of the slot area as well as the armature current capability. The shape of the stator slot has a critical impact on the MG effect as well as the turns of the copper wires.

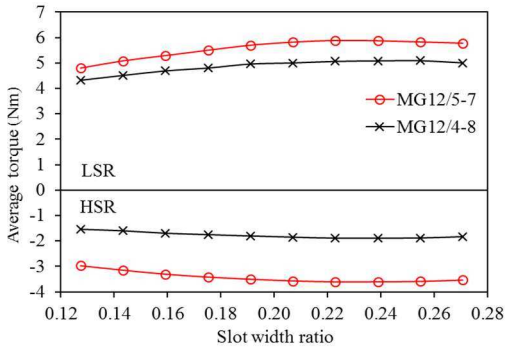

Fig. 7 Influence of slot width on average torque.

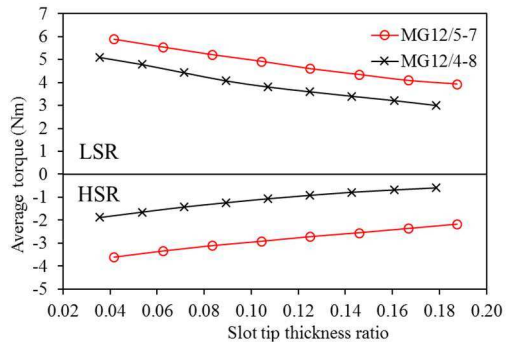

Fig. 8 Influence of slot tip thickness on average torque.

D. *Influence of slot opening width*

The influence of the slot opening width on the average torque is obtained by studying the changing of the ratio of the stator pole width w_{st} to the stator pole pitch τ_s. Fig. 9 indicates the effect of slot opening width on both machines

torque performance. It can be noted that the machine torque of the two models reaches its maximum value when the slot opening ratio is approximately 0.38. This effect is due to the leakage flux between two different pole tips being eliminated as the slot opening increases.

E. Influence of the ratio between outer and inner diameters

The influence of the ratio of the machine inner diameter (ID) with respect to the machine outer diameter (OD) was also studied. The inner diameter is changed at different values whereas the outer diameter is kept constant. Fig. 10 indicates the influence of inner to outer diameter variation on the machine torque performance. It is obvious that the average torque of the two topologies increases as the ratio decreases. On the other hand, when the ratio increases, the machine's active length decreases which results in decreasing of the stator coil and the magnet lengths.

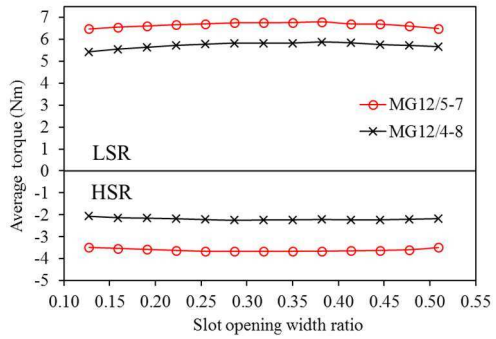

Fig. 9 Influence of slot opening on average torque.

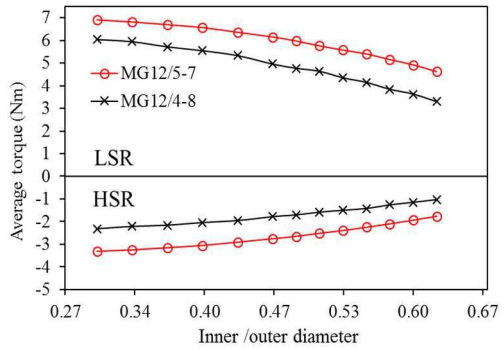

Fig. 10 Influence of machine inner diameter on average torque.

V. Analysis of Proposed Magnetically Geared Machine.

Both MG12/5-7 and MG12/4-8 are analyzed and studied in this section. With two machine specifications and parameters listed in Table II, the no-load performance is calculated at zero relative angle between the HSR and LSR pole axes. However, with the aim of calculating the torque performance and obtaining maximum MG torque, the axes of both rotors are placed to have a relative position angle of 90 elec. deg. [28]. With stationary modulator pieces, the relative electrical angle δ between two rotors can be calculated by

$$\delta = p_h\theta_h - p_l\theta_l \tag{7}$$

where θ_h and θ_l are the mechanical axis angles of HSR and LSR, respectively. The maximum relative position angle is obtained by fixing the LSR pole axis at zero initial position, whereas the HSR axis position is rotated over 90 elec. deg. (18 mech. deg. of MG12/5-7, and 22.5 mech. deg. of MG12/4-8) with the reference of LSR position, as explaind in Fig. 11. By utilizing 3D-FEA, the performance of the machine is verified and compared at no-load and on-load conditions.

A. No-load field and back-EMF

The no-load performance is firstly obtained and compared for both machines. Fig. 12 plots the no-load flux density distributions of both machine geometries at initial position. It can be seen that the flux density of the MG12/5-7 is higher than that of the MG12/4-8. Moreover, the machine is simulated at open circuit and both rotors are rotating at their rated speeds. The no-load performance is calculated at initial relative angle between HSR and LSR being zero, in which the d- axis of HSR and LSR poles are aligned. Fig. 13 shows the comparison of phase flux linkages for both AFMGPM machines. It can be observed that the phase flux linkage waveforms of the two machines are sinusoidal and symmetrical. Also, it is clear that MG12/5-7 has higher flux linkage magnitude of approximately 17.2 mWb, whereas MG12/4-8 has flux linkage magnitude of approximately 15.3 mWb.

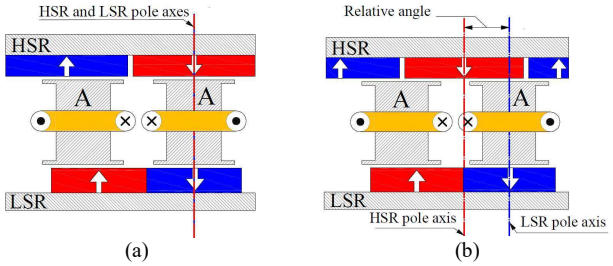

Fig. 11 Illustration of relative angle between HSR and LSR. (a) Minimum relative angle (0 elec. deg.). (b) Maximum relative angle (90 elec. deg.).

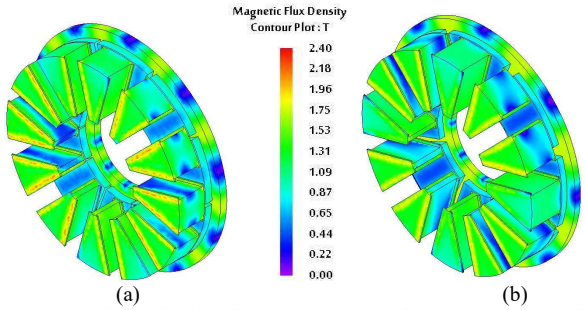

Fig. 12 No-load flux density distributions at initial position. (a) MG12/5-7 (b) MG12/4-8.

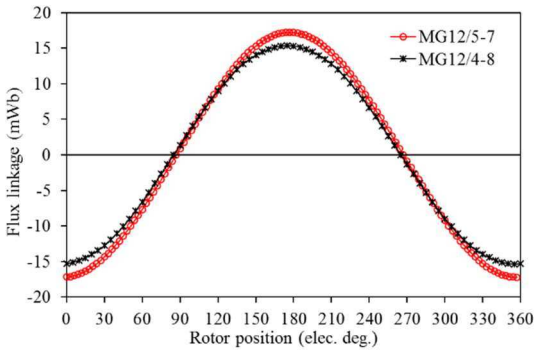

Fig. 13 Comparison of no-load flux linkages for different rotor pole combinations at zero relative angle.

The phase back EMFs and the corresponding spectra of the proposed topologies are compared in Fig. 14. It shows that both machines contain slight 3rd and 5th harmonics. On the other hand, the back EMF induced in the stator windings is a result of the summation of the back EMF produced by both rotors. The back EMF amplitude values of MG12/5-7 and

MG12/4-8 are approximately 3.6 and 2.6 V, respectively. Moreover, the comparison indicates that MG12/5-7 has significant higher EMF amplitude in that the machine back EMF is proportional to the winding factor which is higher than MG12/4-8 as evidenced in Table I.

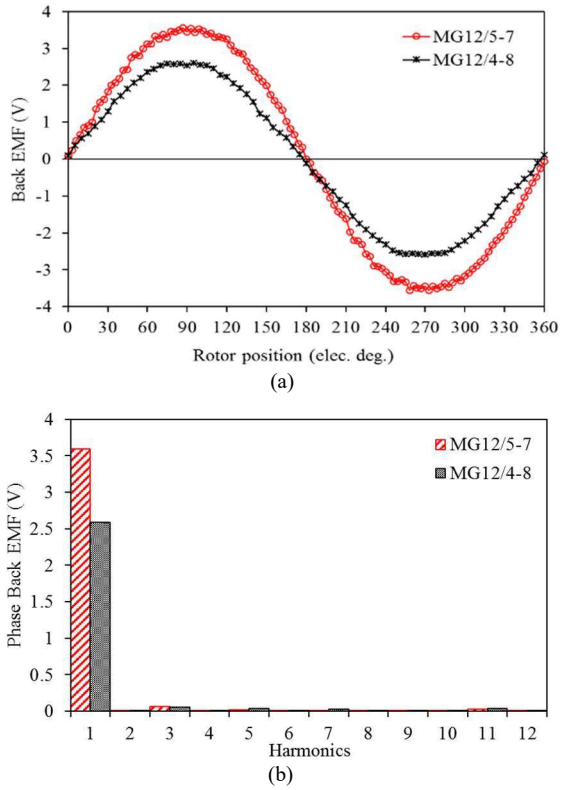

Fig. 14 Comparison of no-load phase back EMFs and corresponding harmonics at zero relative angle. (a) Waveforms (b) Harmonics spectra.

B. *Torque*

The torque of the proposed machine consists of two parts: torque produced by MG effect, which is a function of the relative position between HSR and LSR, and electromagnetic torque produced by the interaction of armature field and PM field. Fig. 15 shows the MG torque angle characteristics for the proposed machine which can be obtained by blocking the LSR at initial position of $\theta_l = 0^o$ whereas the HSR is incrementally rotated with the reference of the LSR position. It is clear that the torque of both rotors increases as the relative angle increases and reaches its maximum value when δ is 90 elec. deg., in which the corresponding mechanical angles of HSRs θ_h of MG12/5-7 and MG12/4-8 are 18° and 22.5°, respectively. Similarly, by holding the HSR still at $\theta_h = 0^o$ and rotating the LSR with reference of the HSR initial position, the torque reaches its maximum value when the corresponding mechanical angle of LSRs θ_l of MG12/5-7 and MG12/4-8 are 12.85° and 11.25°, respectively. In fact, the angle between the HSR and LSR is determined by the applied load. In other words, when no load is applied on the output shaft, the relative angle is approximately zero if the torque produced by the rotor weight is neglected. Moreover, as the load increases, the relative angle increases and the torque reaches its maximum value when the relative angle is 90 elec. deg. Further, when the load exceeds the maximum torque value, both rotors will slip. Moreover, Fig. 16 shows the MG effect torque performance and the harmonics spectra for both topologies when the relative angle is adjusted at 90 elec. deg (Mode 1). For the proposed MG12/5-7, the maximum torques for HSR and LSR are approximately 3.83 Nm and 5.34 Nm respectively, and the corresponding magnetic gear ratio of approximately 1.40 can be obtained. Moreover, for the proposed MG12/4-8, a maximum torque of approximately 2.24 Nm and 4.49 Nm can be obtained by HSR and LSR respectively, in which the gear ratio is approximately 2.0. In addition, MG12/4-8 has more torque ripple compared to MG12/5-7. The effect of machine torque ripple can be explained and predicted by the cogging torque factor C_T, which can be presented by the formula given in [29]:

$$C_T = \frac{2p\ N_s}{LCM\ (2p,N_s)} \tag{8}$$

where $LCM\ (2p, N_s)$ is the least common multiple between the number of stator poles and the number of poles of either HSR or LSR. The higher C_T value indicates higher torque ripple value; however, the minimum value for C_T is unity which constitutes a proper selection for rotor pole pair combinations. Consequently, the torque ripple exhibited in the proposed machine can be estimated. It is obvious that C_T is 2 for both HSR and LSR of MG12/5-7, and, similarly, C_T factors of MG12/4-8 for both rotors are 4.

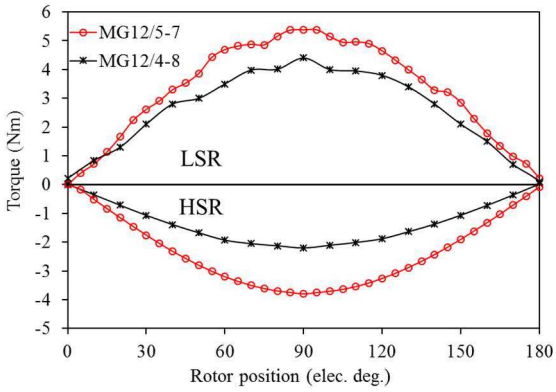

Fig. 15 MG effect torque-HSR angle characteristics for HSR and LSR with the reference of LSR.

Moreover, Fig. 17 shows that when the rated current is applied to the stator winding, the LSR torques for both machines increase (Mode 2). However, the average HSR torque will not be affected by armature reaction current. According to operation principles of synchronous machines, the d- axis of the LSR flux is aligned with the phase A pole as shown in Fig. 11. Therefore, the armature field only interacts with the PM field of LSR, which results in extra torque and torque being transferred from HSR due to the gearing effect. Fig. 18 shows the relationship between the machine average torque and the current angle at the optimal relative angle. It is obvious that the torque produced by armature reaction can be controlled by the current angle. On the other hand, the power/torque produced by the armature reaction can be split between the high and low-speed rotors by changing the current angle between (0 and 90) elec. deg. In this case, the armature reaction flux is aligned with LSR PM flux. In addition, by changing the current angle to its optimal value of 90 elec. deg., the armature current torque will be added to HSR torque. Furthermore, at maximum torque exerted on a specific rotor, the armature reaction effect on the other rotor should be zero. In general, the matching between MG torque of either HSR or LSR and armature reaction torque can be obtained by the accurate choice of the stator's current angle at the given relative angle.

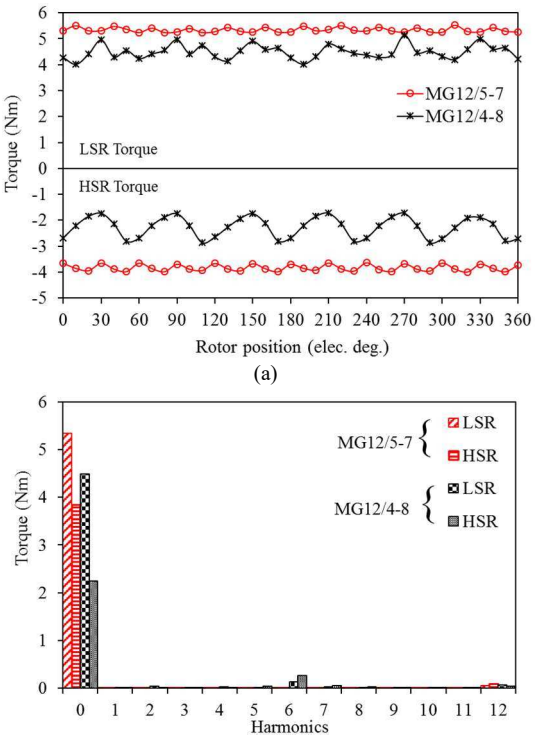

Fig. 16 Comparison of high and low-speed rotor MG torques for different rotor pole combinations (a) Torques. (b) Spectra.

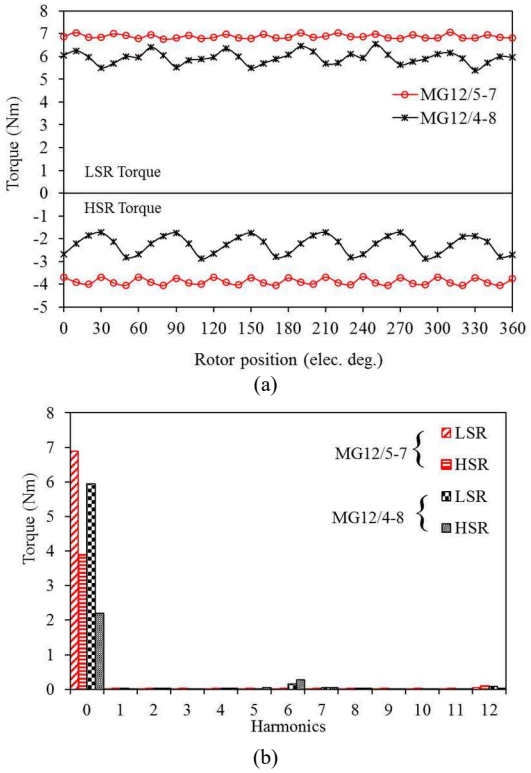

Fig. 17 Comparison of high and low speed rotor torques for different rotor pole combinations at full load (a) Torques. (b) Spectra.

C. *Axial force*

The major force which should be considered in the machine analysis is the attractive force between the rotor PMs and the stator core (the axial force). Fig. 19 compares the axial forces exerted on the machine rotors at no-load and on-load conditions. It is worth mentioning that the force is calculated at maximum relative angle between HSR and LSR (90 elec. deg.). In this case, the d-axis of the LSR and the d-axis of phase A are aligned, whereas the HSR is adjusted at 90 elec. deg. with the reference of the LSR. It can be seen that the average magnetic forces of HSR and LSR are unequal due to the unequal number of rotor poles and hence different air-gap flux density. Moreover, the magnetic forces applied on the HSRs are slightly increased at on-load condition due to the armature current flux density, whereas the forces applied on the LSRs are approximately the same as that at no-load condition since the d-axis of the LSR and the axis of phase A are aligned. Moreover, as can be seen in Fig. 20, an unbalanced force exists on the machine stator since the force on the stator is the sum of both rotor forces, but in opposite directions.

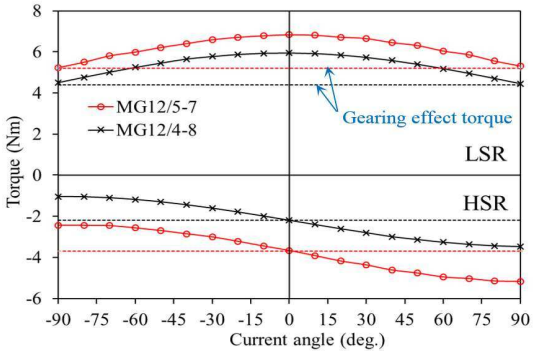

Fig. 18 Torque – current angle curves at maximum MG torque.

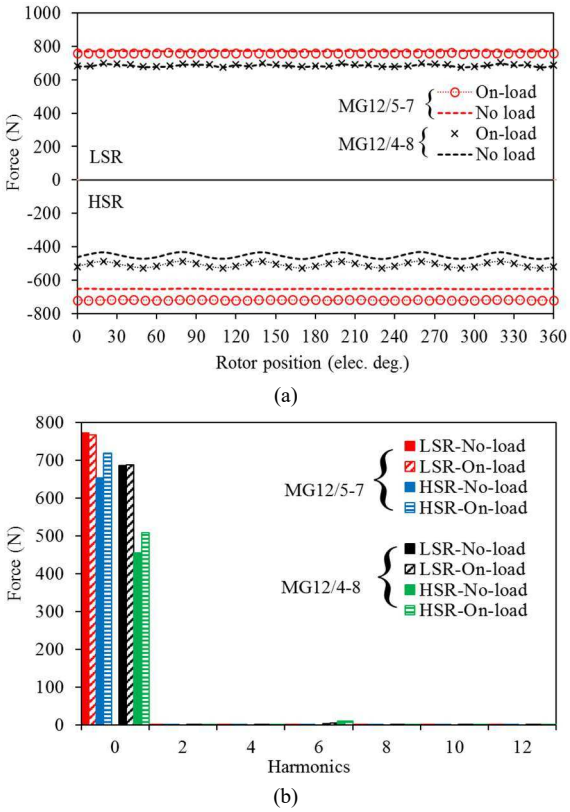

Fig. 19 Comparison of high and low speed rotor axial forces for different rotor pole combinations at no-load and on-load. (a) Axial forces. (b) Spectra.

D. *Losses and efficiency*

With the aid of JMAG 3D-FEA, the losses within the stator and the rotor of the proposed machine topologies are analyzed and compared. Assuming constant copper loss of 30 W and constant rated rotor speeds at the maximum relative angle of 90 elec. deg., the iron loss is evaluated when the LSR is considered as an output torque. Moreover, in order to estimate the magnet eddy current loss, the magnet characteristics are assumed to be linear. A magnet permeability (μ_r) of 1.05 and

a magnet resistivity of 1.4×10^{-5} (Ωm) are assigned to the magnet. Furthermore, at rated rotor speeds and when the mechanical loss is ignored, the efficiencies of both topologies are calculated and compared. Table IV compares the losses, efficiencies and power factors of the two topologies. It is evident that the PM and iron losses are higher in MG12/5-7 since both the flux density and the output torque are higher. However, MG12/5-7 has higher efficiency compared with MG12/4-8 at the given copper loss.

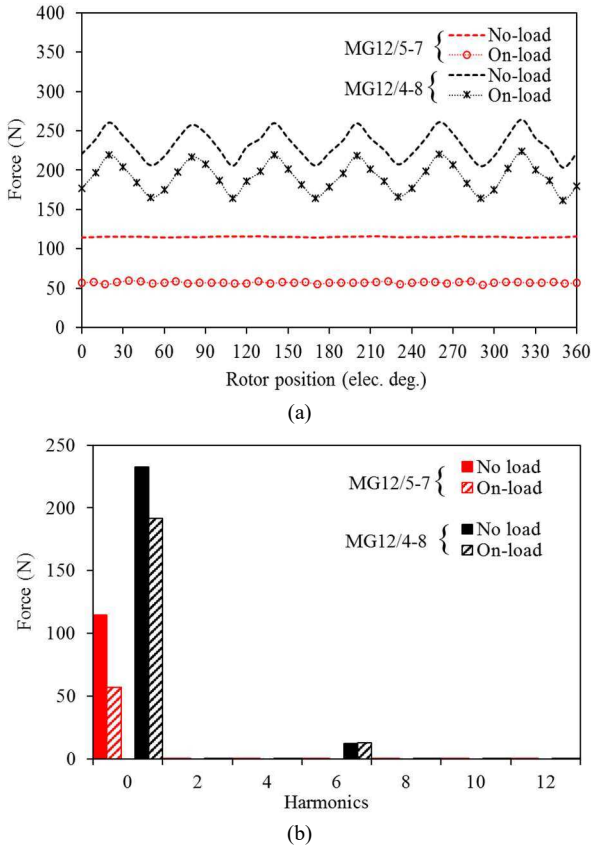

Fig. 20 Comparison of axial forces applied on stators for different rotor pole combinations at no-load and on-load. (a) Axial forces. (b) Spectra.

TABLE IV
COMPARISON OF MACHINE LOSSES AND EFFICIENCY AT RATED CURRENT AND SPEED

Parameter	MG 12/5-7	MG 12/4-8
LSR speed (rpm)	285.7	200
Torque density (Nm/m^3)	43	37.5
Mechanical output power (W)	203.5	124
Copper loss (W)	30	30
PM eddy current loss (W)	0.34	0.3
Iron loss (W)	2.8	2.2
Power factor	0.7	0.54
Efficiency (%)	86	79.2

E. Influence of machine size on power output

In addition to HEVs, the presented machine in this study is also suitable for other low speed high torque applications, such as wind power generation [30] [31]. For the machine mentioned above, the output power at rated speed is quite low since its outer diameter is very small. Therefore, the influence of the machine size and the possibility for higher power applications will be discussed in this sub-section. From the conventional AFPM machine point of view, it is evident that the outer diameter has a significant impact on the machine torque/power at constant speed since they are proportional with the cube of the outer diameter ($T \propto D_O{}^3$) [20]. In addition, it is obvious that with the increase of the machine size, the optimal modular (slot)/rotor pole number combination and geometrical structure for largest output power changes. However, for the sake of simplicity and discussion, the proposed MG12/5-7 machine is simply scaled up since it has a larger output power than the MG12/4-8. The optimized topology of MG12/5-7 is scaled in both radial and axil directions with the same scale factor as explained in Fig. 21. Fig. 22 indicates the powers of the HSR and LSR and the corresponding machine volume at different scale factors at the rated speeds. It is clear that the machine volume linearly increases with the scale factor, and power significantly increases as the machine is scaled up. Therefore, according to the obtained results, when the outer diameter and the axial length are scaled by 10, (i.e. D_o=900 mm and L_x=250 mm), the input and the output power of 206 kW and 157 kW can be predicted, respectively.

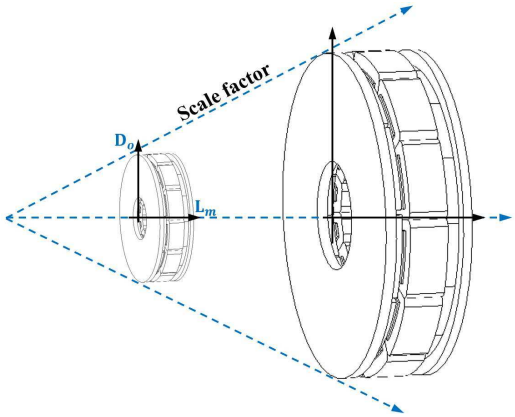

Fig. 21 Volume scale method of the proposed topology.

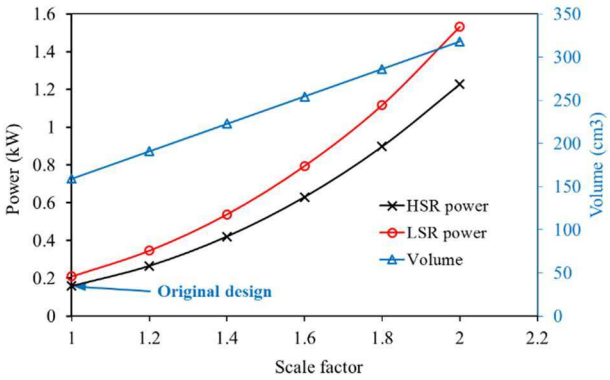

Fig. 22 Influence of machine volume on output power at rated speed.

VI. PROTOTYPE DESIGN AND RESULT VALIDATION

In order to validate the FEA results, a prototype machine consisting of 12 stator poles made of laminated steel, a 10-pole high speed PM rotor (HSR) and a 14-pole low speed PM rotor (LSR) was fabricated and tested. For the sake of manufacturing simplicity, the magnets and the stator pieces were made to be rectangular as can be seen in Fig. 23. The main design parameters are listed in Table V. On the other hand, using the same prototype dimensions, an FE model is established and simulated with the aid of 3D-FE software. The prototype was tested at no-load to calculate the cogging torque, static MG torque and back-EMF. Moreover, the on-load static torque at half load and full load currents was measured and compared with the predicted results.

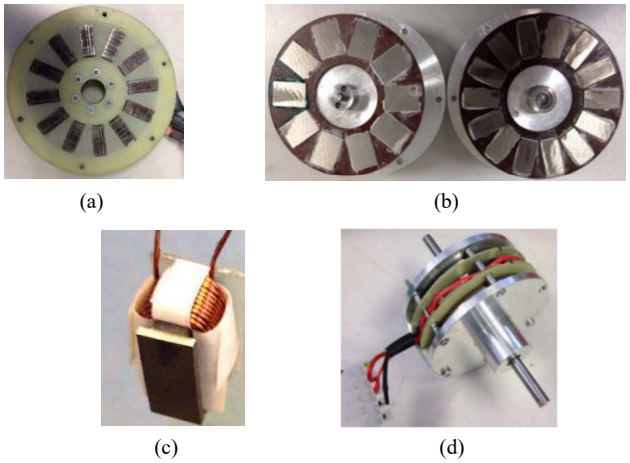

(a) (b) (c) (d)

Fig. 23 The machine prototype. (a) Stator, (b) Rotors (c) Stator pole. (d) The assembled machine prototype.

TABLE V
THE PROTOTYPE DIMENSIONS AND PARAMETERS.

Parameter	Value	Parameter	Value
HSR pole pair no. (p_h)	5	LSR pole width (mm)	10
LSR pole pair no. (p_l)	7	LSR pole height (mm)	20
No. of stator slot (n_s)	12	Rotors back iron thickness (mm)	3
No. of coils /phase	4	Stator pole height (mm)	20
No. of turns /phase	168	Coil diameter (mm)	0.71
Air-gap width (mm)	0.5	Winding resistance /phase (Ω)	0.5
Axial length (mm)	30	Winding inductance /phase (mH)	0.54
Stator (ID) (mm)	48	Packing factor	0.5
Stator (OD) (mm)	88	Max. rated current (A)	6
HSR pole thickness (mm)	3	Gearing ratio G_r	1.4
HSR pole width (mm)	14	Magnet material	N35SH
HSR pole height (mm)	20	PM remanence B_r (T)	1.21
LSR pole thickness (mm)	3.5	Iron material	Mild steel

A. Cogging torque

The individual cogging torques of HSR and LSR were firstly measured utilizing the measuring method described in [32] and with the aid of the test rig shown in Fig. 24. One rotor shaft was connected to a balance beam to measure the force produced by the prototype with the aid of a digital weight scale while the other rotor was able to freely rotate. The stator was fixed to the lathe machine which could be freely rotated to vary the rotor position. Moreover, a pre-load weight was located on the beam above the digital scale to keep continuous attachment with the digital scale when the position was changed. By changing the stator angular position, the cogging torque at different rotor positions could be measured for each rotor.

Fig. 25 shows the measured and predicted LSR cogging torques for the proposed magnetically geared machine. Similarly, Fig. 26 shows the measured and predicted HSR cogging torques. It is obvious that the predicted cogging torques of LSR and HSR are relatively small. Moreover, since the magnet shape has been changed for manufacturing consideration, the machine cogging torque is expected to be changed. It is clear that utilizing rectangular magnet reduces the LSR cogging torque amplitude, whereas the cogging torque of the HSR is significantly increased by utilizing a rectangular magnet shape as shown in Fig. 25 and Fig. 26, respectively. The discrepancy between FEA and tested results is caused by manufacturing tolerances.

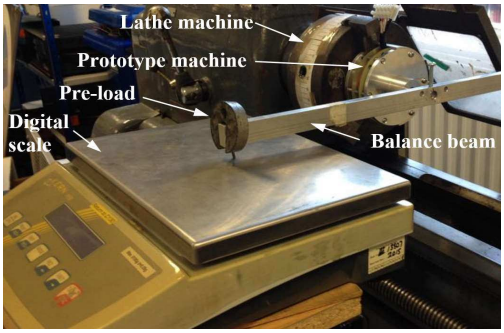

Fig. 24 Test rig for static torque measurement.

B. Phase back-EMF

The measured and predicted phase back EMF are compared and plotted in Fig.27. The HSR was driven by a 400 rpm prime-mover; therefore, an approximate 285 rpm is measured for the speed of LSR. It shows that the measured and predicted back-EMF amplitudes are approximately 5.9V and 6.2V, respectively, in which a good validation is obtained, and the difference between the measured and the predicted EMF amplitudes is mainly attributed to the manufacturing imperfection.

C. No-load and on-load torques

The measured and predicted LSR and HSR static MG torques are compared in Fig. 28. The MG torque can be measured by applying forces to the HSR shaft and measuring the corresponding LSR forces with the aid of a digital scale. It is obvious that, at no-load, the machine MG torque is zero at the initial position since the relative angle between HSR and LSR is zero elec. deg. In addition, the MG torque for the LSR rotor increases with the relative angle and it reaches maximum when the relative angle between the two rotors equals 90 elec. deg. Moreover, according to the obtained LSR and HSR torques, it is confirmed that the magnetic gear ratio for the prototype is approximately 1.40.

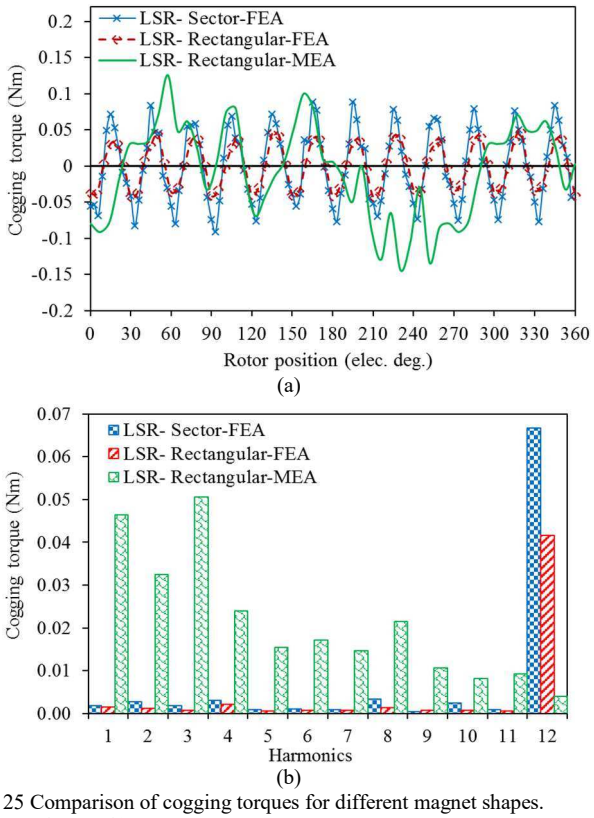

Fig. 25 Comparison of cogging torques for different magnet shapes. (a) Waveforms. (b) Spectra.

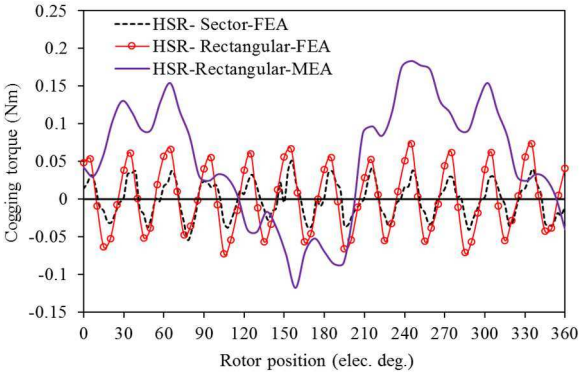

(a)

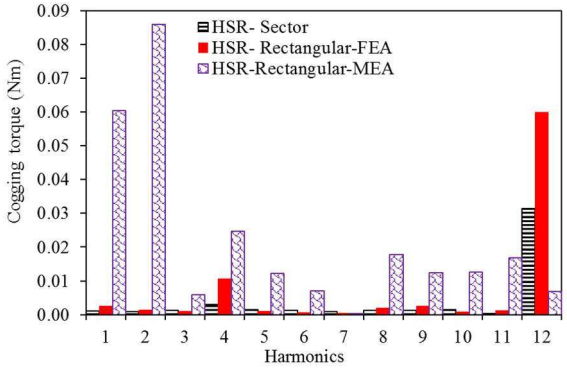

(b)

Fig. 26 Comparison of HSR cogging torques at different magnet shape. (a) Waveforms. (b) Spectra

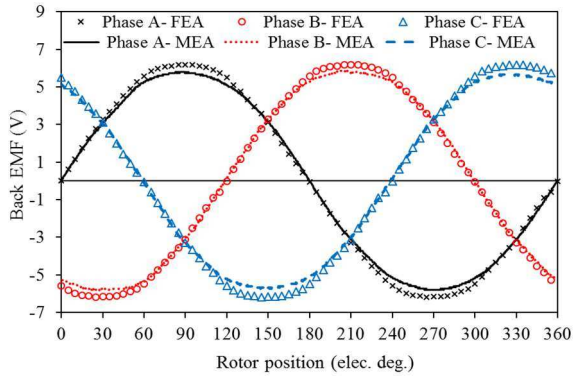

(a)

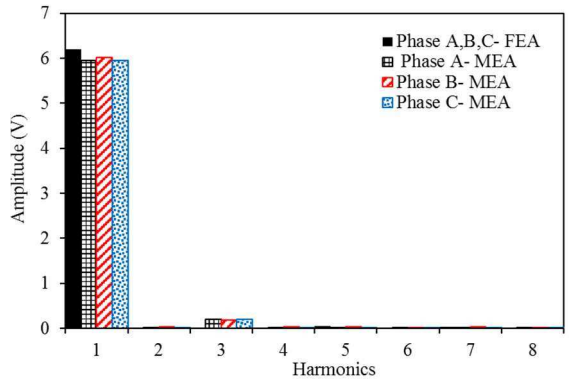

(b)

Fig.27 Comparison of 3-phase back EMFs at 400 rpm. (a) Waveforms. (b) Spectra.

The on-load static torque is measured utilizing the same measuring method of cogging torque described in [32] and with the aid of the test rig displayed in Fig. 24. To do this, one rotor was fixed in place to the stator with a clump which is fixed to a lathe machine. Moreover, the other rotor shaft is connected to a balance beam to measure the force produced by the prototype with the aid of digital weight scale. In this case, the rotor will be stationary whereas the fixed rotor and the stator are rotated to vary the rotor position. Subsequently, by supplying the stator windings with DC currents ($I_a=I$, $I_b=I_c=-½I$), the prototype on-load static torque can be measured. Furthermore, it should be mentioned that to obtain maximum on-load LSR static torque, the d- axis of the HSR pole and the phase A stator pole should be aligned as indicated in Fig. 29.

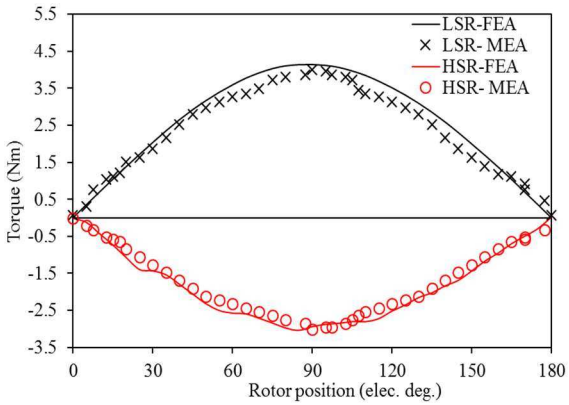

Fig. 28 Comparison of predicted and measured no-load MG static torques of HSR and LSR.

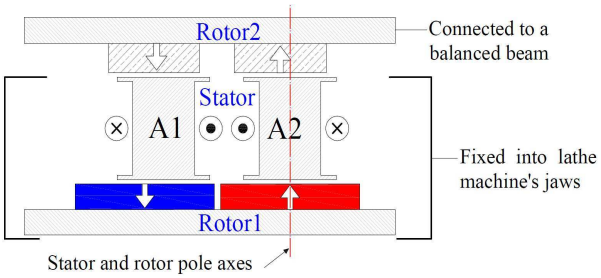

Fig. 29 Stator and rotor connection and alignment for static torque measurement.

The measured and predicted LSR static torques at different stator currents are compared in Fig. 30. When the stator winding is fed by specific current, an electromagnetic torque can be obtained and the machine torque increases further as the LSR position increases. The measured and predicted LSR torque constants are 0.18, and 0.19, respectively. Similarly, a comparison between the measured and the predicted HSR static torques at different stator currents are shown in Fig. 31. In this case, the LSR is fixed with the stator whereby the HSR torque is measured. The measured and predicted HSR torque constants are approximately 0.15. A good validation between measured and simulated results is therefore obtained.

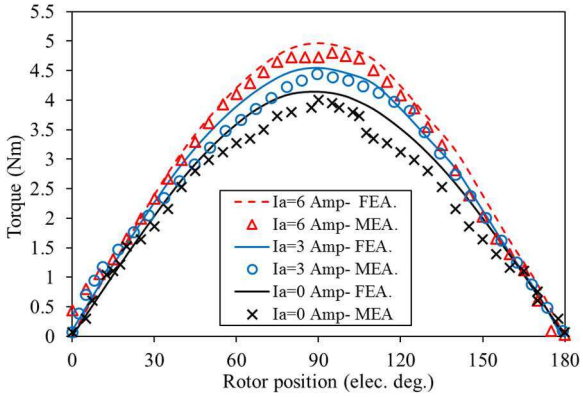

Fig. 30 Comparison of predicted and measured LSR static torques at different currents.

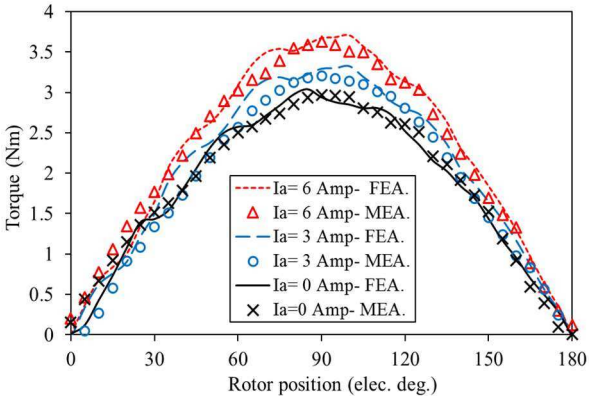

Fig. 31 Comparison of predicted and measured HSR static torques at different currents.

VII. Conclusion

In this study, a new axial flux magnetically geared machine for power split applications is presented. Combining an axial magnetic gear with a PM machine results in a new magnetically geared machine which is capable of splitting or mixing the machine input powers. Furthermore, various operating modes of the proposed topologies are studied and investigated. It has been shown that the mechanical input torque applied on either the HSR or the LSR can be scaled up or down by utilising the proposed AFMGPM. Moreover, the output torque transferred by magnetic gearing effect can be increased by the armature reaction torque. The performance comparisons between MG12/5-7 and MG12/4-8 show that both topologies have significant torque density at no-load and on-load conditions. Nevertheless, MG12/4-8 has lower torque and higher torque ripple compared to MG12/5-7. In general, the machine performance investigation states that at specific relative angle of two rotors, the torque produced by the armature current can be controlled by the machine's current angle. In addition, the proposed machine has been designed, prototyped and tested. Overall, the prototype confirms the proposed machine's operation principle and the measured results show a good agreement with the predicted results.

References

[1] M. Aydin, H. Surong, and T. A. Lipo, "A new axial flux surface mounted permanent magnet machine capable of field control", *IEEE Ind. Appl. Conf.*, 2002, pp. 1250-1257.

[2] D. E. Hesmondhalgh, D. Tipping, "A multielement magnetic gear", *IEE Pro. Elec. Power Appl.,* vol. 127, no. 3, pp. 129-138, May1980.

[3] K. Atallah and D. Howe, "A novel high-performance magnetic gear", *IEEE Trans. Magn.*, vol. 37, no.4, pp. 2844-2846, Jul 2001.

[4] P. M. Tlali, R. J. Wang, and S. Gerber, "Magnetic gear technologies: A review", *Int. Conf. on Elec. Mach. (ICEM)*, 2014, pp. 544-550.

[5] M. Ehsani, Y. Gao, and J. M. Miller, "Hybrid Electric Vehicles: Architecture and Motor Drives", *in Proc. IEEE*, vol. 95, no.4, pp. 719-728, April 2007.

[6] J. M. Miller, "Hybrid electric vehicle propulsion system architectures of the e-CVT type", *IEEE Trans. on Power Electronics*, vol. 21, no.3, pp. 756-767, May 2006.

[7] K. Atallah, J. Rens, S. Mezani, and D. Howe "A novel "pseudo" direct-drive brushless permanent magnet machine", *IEEE Trans. Magn.*, vol. 44, no.11, pp. 4349-4352, Nov.2008.

[8] L. Jian, "Electromagnetic design and analysis of a novel magnetic gear integrated wind power generator using time stepping finiteelement method," *Prog. Electromagn. Res.*, vol. 113, pp. 351-367, Feb.2011.

[9] L. Jian and K. T. Chau, "Design and analysis of a magnetic-geared electronic-continuously variable transmission system using finite element method", *Prog. Electromagn. Res.,* vol. 107, pp. 47-61, 210, July 2010.

[10] S. Niu, S. L. Ho, and W. N. Fu, "Design of a novel electrical continuously variable transmission system based on harmonic spectra analysis of magnetic field," *IEEE Trans. Magn.*, vol. 49, no.5, pp. 2161-2164, May 2013.

[11] N. Niguchi, K. Hirata, A. Zaini, and S. Nagai, "Proposal of an axial-type magnetic-geared motor", *in Proc, 20th Int. Conf. Elect. Mach.*, 2012, pp. 738-743.

[12] R. J. Wang, L. Bronn, S. Gerber, and P. M. Tlali, "Design and evaluation of a disc-type magnetically geared PM wind generator", *4th Int. Conf. Power Eng., Energy and Elect. Drives*, pp. 1259-1264.May 2013.

[13] H. Zaytoon, A. S. Abdel-khalik, A. M. Massoud, and S. Ahmed, "An axial magnetic gearbox with an electric power output port", *29th Annual IEEE App. Power Electronics Conf. Expo.*, 2014, pp. 2621-2627.

[14] M. Johnson, M. C. Gardner, and H. A. Toliyat, "Design and analysis of an axial flux magnetically geared generator", *IEEE Energy Conv. Congr. Expo. ,* 2015, pp. 6511-6518.

[15] J. Lai, J. Li, R. Qu, R. Zhang, and D. Li, "A novel axial flux magnetic-field-modulated dual-mechanical-port dual-electrical-port machine for hybrid electric vehicle", *IEEE Vehicle Power and Propulsion Conf. (VPPC)*, 2016, pp. 1-6.

[16] S. Niu, Y. Liu, S. L. Ho, and W. N. Fu, "Development of a novel brushless power split transmission system for wind power generation application", *IEEE Trans. Magn.*, vol. 50, no. 11, pp. 1-4, Nov. 2014.

[17] C. Tong, Z. Song, P. Zheng, J. Bai, and Q. Zhao, "Research on electromagnetic performance of an axial magnetic-field-modulated brushless double-rotor machine for hybrid electric vehicles", *17th Int. Conf. on Elec. Mach. Sys. (ICEMS)*, 2014, pp. 2896-2902.

[18] M. F. H. Khatab, Z. Q. Zhu, H. Y. Li, and Y. Liu, "Optimal design of a novel axial flux magnetically geared PM machine", *Twelfth Inter. Conf. on Ecolo.Vehi. and Renewable Energies (EVER)*, 2017, pp. 1-8.

[19] Z. Q. Zhu, M. F. H. Khatab, H. Y. Li, and Y. Liu, "A novel axial flux magnetically geared machine for power split application", *Twelfth Int.Conf. Ecolo. Vehicles and Renewable Energies (EVER)*, 2017, pp. 1-8.

[20] T. J. Woolmer and M. D. McCulloch, "Axial flux permanent magnet machines: A new topology for high performance applications", *IET Hybrid Vehicle Conf.*, 2006, pp. 27-42.

[21] Qinfen Lu, Huanwen Li, Xiaoyan Huang, Yunyue Ye, "Research on yokeless double-sided multi-tooth flux-switching linear motor", *COMPEL*, vol.35, no.2, pp.832- 843, 2016.

[22] Corporation, JMAG : Simulation Technology for Electromechanical Design.. Available at: https://www.jmag-international.com.

[23] K. Atallah, S. D. Calverley, and D. Howe, "Design, analysis and realisation of a high-performance magnetic gear", *IEE Proc., Elec. Power Appl.*, vol. 151, no. 2, pp. 135-143, Mar.2004.

[24] D. Ishak, Z. Q. Zhu, and D. Howe, "Permanent magnet brushless machines with unequal tooth widths and similar slot and pole numbers", *IEEE Trans. Ind. Appl.,* vol.l41, no. 2, pp. 584-590, March/April 2005.

[25] J.B. Wang, K. Atallah, Z. Q. Zhu, and D. Howe, "Modular three-phase permanent-magnet brushless machines for in-wheel applications", *IEEE Trans. on Vehicular Tech.,* vol. 57, no. 5, pp. 2714-2720, Sep.2008.

[26] J. Cros and P. Viarouge, "Synthesis of high performance PM motors with concentrated windings", *IEEE Trans. on Energy Conv.,* vol. 17, no. 2, pp. 248-253, June 2002.

[27] A. Du, X. Yu, and J. Song, "Structure design for power-split hybrid transmission", *Int. Conf. on Mechatronics and Automation (ICMA)*, 2010, pp. 884-887.

[28] N. W. Frank and H. A. Toliyat, "Gearing ratios of a magnetic gear for wind turbines", *in Proc. IEEE int. Elec. Mach. Drives Conf.*, 2009, pp. 1224-1230.

[29] Z. Q. Zhu and D. Howe, "Influence of design parameters on cogging torque in permanent magnet machines", *IEEE Trans. on Energy Conv.,* vol. 15, no. 4, pp. 407-412, Dec. 2000.

[30] X. Sun, M. Cheng, L. Xu, and W. Hua, "A novel dual power flow wind power generation system," *in Proc. Int. Conf. Electr. Mach. Syst.*, Wuhan, China, 2008, pp. 2573–2578.

[31] X. Luo and S. Niu, "A novel contra-rotating power split transmission system for wind power generation and its dual MPPT control Strategy", *IEEE Trans. on Power Electronics*, vol. 32, no. 9, pp. 6942-6935, Sep. 2017.

[32] Z. Q. Zhu. "A simple method for measuring cogging torque in permanent magnet machines", *in Proc. IEEE . power & Energy Society General Meeting (PES)*, Calgary, 26–30, July 2009; pp. 1–4.

Z. Q. Zhu (M'90–SM'00–F'09) received the B.Eng. and M.Sc. degrees from Zhejiang University, Hangzhou, China, in 1982 and 1984, respectively, and the Ph.D. degree from The University of Sheffield, Sheffield, U.K., in 1991, all in electrical and electronic engineering.

Since 1988, he has been at The University of Sheffield, where he currently holds the Royal Academy of Engineering/Siemens Research Chair and is the Head of the Electrical Machines and Drives Research Group, the Academic Director of Sheffield Siemens Wind Power Research Centre, the Director of Sheffield CRRC Electric Drives Technology Research Centre, and the Director of Midea Electric Machines and Controls Research Centre. His research interests include the design and control of permanent-magnet machines and drives for applications ranging from automotive through domestic appliances to renewable energy.

Prof. Zhu is a Fellow of Royal Academy of Engineering.

Mohammed F. Khatab received the B.S. degree from Omar-Almukhtar (OMU) University, El Bayda, Libya, in 1999 and the M.S. degree from University of Newcastle, Newcastle upon tyne, UK, in 2010, all in electrical and electronic engineering. He is currently pursuing the Ph.D. degree in electrical engineering at University of Sheffield, Sheffield, UK. His research interest includes design and control of permanent magnet and magnetic geared machines.

Hua-Yang Li was born in Shanxi, China, in 1992. He received the B.Eng. and M.Sc. degrees in electrical engineering from Zhejiang University, Hangzhou, China, in 2013 and 2016. He is currently pursuing the Ph. D. degree at University of Sheffield, Sheffield, U.K. His research interests include design of magnetic gears and permanent magnet machines.

Yue Liu (S'16) received the B.Eng. and M.Sc. degrees in electrical and electronic engineering from Harbin Institute of Technology, Harbin, China, in 2013 and 2015, respectively. He is currently working toward the Ph.D. degree in the Department of Electronic and Electrical Engineering, University of Sheffield, Sheffield, U.K.